Spin-flip Raman scattering in semi-magnetic quantum wells with in-plane anisotropy: Analysis of the intermediate states

A. V. Koudinov, Yu. G. Kusrayev, and B. P. Zakharchenya
A. F. Ioffe Physico-Technical Institute, St. Petersburg 194021, Russia

D. Wolverson* and J. J. Davies
Department of Physics, University of Bath, Bath BA2 7AY, United Kingdom

T. Wojtowicz, G. Karczewski, J. Kossut
Institute of Physics, Polish Academy of Sciences, 02-668 Warsaw, Poland
(Received 6 September 2002; published 5 March 2003)

Spin-flip Raman scattering has been studied in $CdTe/Cd_{1-x}Mn_xTe$ quantum well structures which have previously been demonstrated to possess a reduced symmetry, leading to a hole g tensor which is highly anisotropic in the plane. This unusual behavior has been exploited to investigate in detail the spin-flip Raman-scattering mechanisms. Distinct signals arising from localized excitons and from excitons bound to neutral donors are observed. These signals are found to vary in intensity depending on the angle between the crystal axes and the in-plane magnetic field. The intensities of the signals as a function of laser energy have also been determined. From these observations, a model involving the nature of the intermediate states in the scattering process has been developed which allows the determination of the components of hole g tensor. This model is further applied to explain the observed angular dependence of the spin-flip Raman scattering of the $3d^5$ electrons of the Mn^{2+} ions. In addition, the model predicts a combined scattering process involving both a Mn^{2+} electron and a donor-bound electron; this process is indeed observed.

DOI: 10.1103/PhysRevB.67.115304 PACS number(s): 78.30.−j, 78.67.De

I. INTRODUCTION

The spin properties of electrons in semiconductors have attracted attention over many years. One reason for this is that the effective electron g factors of conduction and valence bands are related to the basic band-structure parameters (such as the interband momentum matrix element) that also determine transport properties and optical transition strengths. A further reason is that, in quantum structures, the electron and hole g factors and their anisotropy contain additional information about carrier confinement, barrier penetration and, as is of interest here, about any reduction of symmetry in the structure.

Among semiconductors, those that are semi-magnetic form a special class since the exchange interactions between carriers in band states and transition-metal ions such as Mn^{2+} lead to large enhancements of the carrier spin splittings in an external magnetic field.[1] As a result, the effects of carrier confinement and of reduced symmetry in quantum structures can then often be investigated with very high sensitivity. In addition, semimagnetic semiconductors are currently of great interest since they can lead to the production of highly spin-polarized carrier populations, for which several types of applications have been proposed. These include devices in which optical recombination is modulated through exploitation of the spin selection rules, as well as devices in which information is manipulated using the electron spin state as an information bit.

For the particular case of $CdTe/Cd_{1-x}Mn_xTe$ quantum wells grown on GaAs substrates, the effects of strain and of quantum confinement are such as to cause the heavy-hole states to lie at lower energy than the light-hole states. If the growth axis ([001]) is taken as the z direction, the g factors of heavy holes are then usually of the form $g_z = g_\parallel$ (finite) and $g_x = g_y = g_\perp \approx 0$ (where we define the directions x and y to be parallel to $[110]$ and $[1\bar{1}0]$, respectively, in the plane of the quantum well). However, in an earlier publication,[2] a striking and surprising form of anisotropy of the heavy-hole g factor was reported in which it was concluded that, for certain specimens, both g_x and g_y become finite, with equal magnitudes but with opposite signs. This very unusual behavior was revealed through studies of the degree of polarization of the low-temperature photoluminescence in an external magnetic field.

There are several previous reports of in-plane anisotropy in heterostructures, for instance arising from an electron-hole exchange interaction having orthorhombic symmetry in excitons localized at type-II heterointerfaces[3,4] or from the nonequivalence of interface bonds in heterostructures containing no common atoms in alternate layers.[5,6] The combined effects of a type-II interface between layers of different atomic species can produce very marked anisotropy;[7] an example is GaAs/AlAs.[8] Recently, it has been shown that even type-I, common anion heterostructures such as the $CdTe/Cd_{1-x}Mn_xTe$ system studied here can exhibit an in-plane anisotropy in magneto-optical studies;[9] this anisotropy was attributed to anisotropic strain relaxation due to different dislocation mobilities in the $[110]$ and $[1\bar{1}0]$ directions.[10]

In the present paper, we describe spin-flip Raman scattering (SFRS) experiments used as a further test of the conclusions of Ref. 2 and of their consequences. SFRS is a technique ideally suited to such investigations since, unlike photoluminescence and many other forms of magneto-optical spectroscopy, it enables one to probe the spin splitting

of only one carrier type. Further, since the scattering is resonantly enhanced when the laser is tuned to the appropriate excitonic transitions, the technique is highly selective, so that, frequently, different types of scattering centers can be studied separately. We have taken advantage of this selectivity to study both electron and Mn^{2+} spin-flip scattering processes in $CdTe/Cd_{1-x}Mn_xTe$ quantum well structures in order to provide further confirmation of the unusual behavior previously reported and to measure the in-plane g values g_x and g_y.

This paper is organized as follows. After a short description of the experimental methods and an overview of the observed spin-flip Raman spectra, we present a detailed analysis of the mechanisms, the angular dependences and the excitation profiles of the electron spin-flip Raman scattering signals, leading to a reconstruction of the hole g tensor whose unusual structure motivated this work (Sec. IV). We then apply the model that we have developed to the case of spin-flip scattering from the $3d^5$ electrons of manganese ions in the structures (Sec. V). Finally, we show that a combined scattering process involving both an electron of a manganese ion and a donor-bound electron is predicted by our model to be of similar intensity to the signals already discussed; we present data showing that this process is indeed observed (Sec. VI).

II. EXPERIMENTAL DETAILS

In spin-flip Raman scattering, one measures the change in energy of an inelastically scattered photon when the scattering is accompanied by a change in the spin state of the center under study (for discussion of SFRS, see Refs. 11–16). In the present experiments, a Ti-sapphire laser pumped by the green/blue output from an argon ion laser was used to provide resonant excitation and the scattered light was analyzed in a spectrometer with a double subtractive filter stage followed by a final dispersing stage of focal length of 1 m. The light was detected either with a charge-coupled detector array or with a cooled GaAs photomultiplier photon counting system. The specimens were mounted in direct contact with superfluid helium at 1.6 K in a superconducting magnet that provided fields up to 6 T. The Raman spectra were taken in the backscattering mode. Both incident and detected polarizations (circular or linear) could be selected by means of quarter wave plates and linear dichroic polarizers; the polarization sensitivity of the spectrometer was compensated by a polarization scrambler whose correct orientation was established using a light source known to be unpolarized. Photoluminescence (PL) spectra were recorded with the same system.

In taking the SFRS spectra, we used either the Faraday geometry, in which the field was parallel to the direction of light propagation, or the Voigt geometry, in which these two directions were perpendicular. In the Voigt geometry (and with the direction of light propagation parallel to the growth axis) the specimen orientation relative to the field direction could be changed by rotating the sample in its plane, the angle between the field and the [110] direction being specified by ϕ. The specimen could also be rotated about an axis perpendicular to both the magnetic field and the light propagation direction, thus enabling investigations in which the field was inclined to the growth axis at an angle θ intermediate between 0° and 90°, and studies of the evolution of the SFRS spectrum from the Faraday to the Voigt configurations.

The samples were grown by molecular-beam epitaxy on GaAs substrates. They both contained four CdTe wells, separated by 500-Å $Cd_{1-x}Mn_xTe$ barriers, the well widths being 20, 40, 60, and 100 Å. The barrier Mn concentrations were $x=0.3$ for sample A and $x=0.5$ for sample B. Sample A is the sample used in the earlier studies of the photoluminescence polarization properties.[2] In the present paper we shall concentrate on the spectra obtained from the 60-Å wells in both specimens, since these quantum wells (QW's) show the most intense spin-flip Raman scattering and the richest variety of SFRS signals.

III. OVERVIEW OF THE SPIN-FLIP RAMAN SPECTRA

The photoluminescence spectrum from the 60-Å well in specimen A showed two distinctly resolved bands with peak positions about 4 meV apart. The spectrum for the 60-Å well in specimen B is qualitatively similar. Such spectra are typical of $CdTe/Cd_{1-x}Mn_xTe$ quantum wells, as reported previously.[17–21] The higher energy line, denoted X, corresponds to the recombination of excitons which are either free or, more probably, weakly localized at fluctuations of the QW potential; the excitons are formed from the lowest-energy single-particle states of the QW ($1e-1hh$ in conventional notation). The lower energy line, denoted D^0X, is ascribed to excitons bound to neutral donors[22–24] in view of the relatively low electron concentration in the present, nominally undoped samples. In more highly doped samples or under high excitation densities, negatively charged excitons, X^-, may also be formed whose PL transitions are expected to occur in the same region of the spectrum as D^0X.[20,21] In the present paper we shall refer throughout to the lower energy line as being D^0X but note that our consideration of the spin selection rules for SFRS is not affected if X^-, rather than D^0X, is involved.

In Fig. 1 we show the effect of optical excitation with the laser wavelength within the X PL band from specimen A, with a magnetic field B of 2 T in the plane of the quantum well and normal to the direction of light propagation (the Voigt configuration). The spectrum was recorded in the (σ,π) polarization geometry, where the first and second symbols represent the polarizer and analyzer, respectively, and where π and σ imply linear polarization along, and normal to, B. In Sec. VI, we shall discuss results obtained with parallel linear polarizations (π,π) and (σ,σ). The PL band centered at 1.6593 eV is the D^0X luminescence while the X luminescence band forms the background on which the SFRS lines are superimposed.

The sharp lines on either side of the laser line represent SFRS processes with a flip of one or more spins of Mn^{2+} $3d^5$ electrons in the barriers.[1] The observed linewidths are determined by the spectral resolution of the experimental setup, typically around 0.1–0.3 cm^{-1} and are, in our system, limited ultimately by the laser linewidth. The Raman shifts

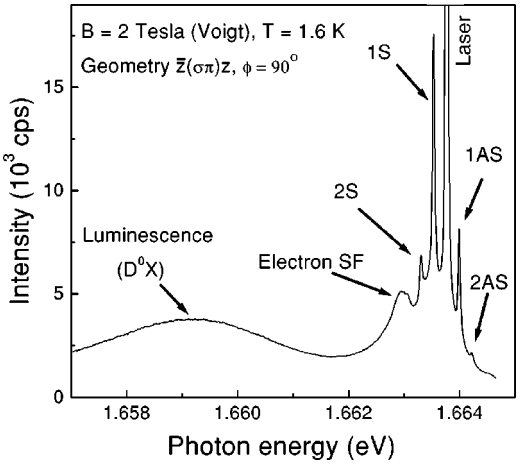

FIG. 1. The photoluminescence and spin-flip Raman scattering spectrum of the 60-Å wide $Cd_{0.7}Mn_{0.3}Te/CdTe$ quantum well of sample A with excitation near the free (or weakly localized) QW exciton transition. The excitation laser line (labeled) is too intense to be represented in the figure. The labels indicate the Stokes (S) and anti-Stokes (AS) Mn^{2+} spin-flip lines, the electron spin-flip signal (electron SF), and the donor-bound exciton photoluminesencence (D^0X)

for these sharp lines increase linearly with the magnetic field as shown in Fig. 2, and for the processes with a spin flip of one manganese $3d^5$ electron (1S, 1AS) correspond to a g factor of 2.00, as expected.[1]

The broader Raman line near 1.663 eV in Fig. 1 corresponds to the spin flip of a conduction-band electron or shallow-donor bound electron. The mechanism of this SFRS process is discussed in more detail in Sec. IV B. As is well-known, the Raman shift of this line is comparatively large even at low magnetic fields but tends to saturation at fields above about 3 T, corresponding to saturation of the paramagnetic Mn^{2+} spin system (Fig. 2).[25] The Mn content of the barriers in the present samples is relatively high and the largest influence on the carriers in a quantum well comes from the Mn^{2+} ions nearest the interfaces to the quantum well; the degree of paramagnetism of these ions is not expected to be typical of bulk $Cd_{1-x}Mn_xTe$ of the barrier composition and it is therefore difficult to model accurately the saturation behavior that we observe. The D^0SF spin-flip line has a Lorentzian line shape with a width of 0.25 meV. This linewidth is independent of the magnetic-field value, suggesting that this is a homogeneous linewidth, in contrast to the PL lines, which are inhomogeneously broadened.

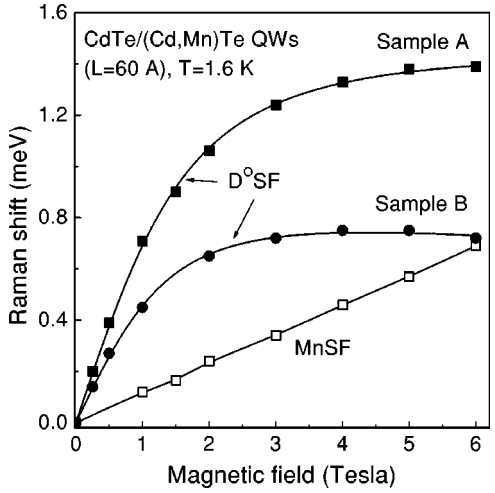

FIG. 2. The dependence of the spin-flip Raman shift on magnetic field in the Voigt geometry for the 60-Å quantum wells of sample A (squares) and sample B (circles). Solid symbols represent signals from the conduction band or shallow-donor bound electron states and open symbols represent Mn^{2+} spin-flip signals. The solid lines represent fits to the data as described in the text.

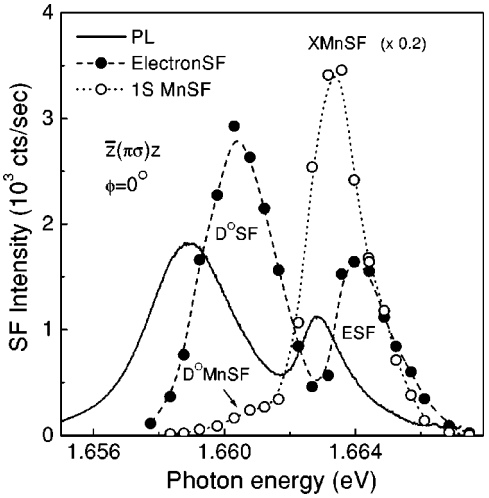

FIG. 3. Spin-flip Raman scattering intensity as a function of excitation energy (''excitation profiles'') for the electron and Mn^{2+} spin-flip signals (filled and open circles, respectively) for sample A in a magnetic field of 2 T in the Voigt configuration, compared to the photoluminescence spectrum of the same sample. The dashed and dotted lines are guides to the eye.

IV. ELECTRON SPIN FLIP

A. Excitation profiles

The intensities of the Raman lines are strong functions of the laser wavelength. In Fig. 3, we show the excitation profiles for the electron and first Stokes Mn^{2+} spin-flip signals in a field of 2 T in the Voigt configuration (the latter is denoted 1S in Fig. 1). A comparison of these profiles with the PL spectrum[26] indicates that it is the QW exciton states which serve here as the intermediate states of the SFRS processes.[1,27,28] The profiles also show that both electron and Mn^{2+} processes can proceed not only via free or weakly localized excitonic states, but also via the impurity-bound excitonic complex D^0X. In both cases, it is the heavy hole components of the excitonic states that are involved.

The key observation of the present work is that, when the polarization geometry of the experiment is changed, the SFRS spectra and their excitation profiles undergo marked and unusual changes. In particular, the spectra obtained in the two geometries, $\bar{z}(\pi,\sigma)z$ and $\bar{z}(\sigma,\pi)z$, are strikingly different; from the symmetry point of view, this is not unexpected since the configurations (π,σ) and (σ,π) are indeed

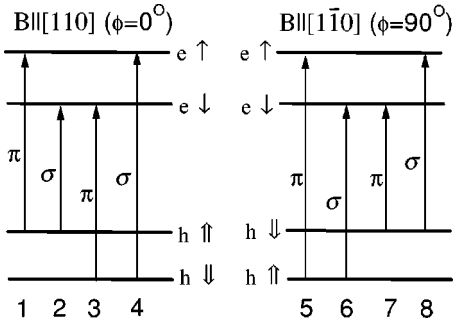

FIG. 4. Key to the model presented in this work: the electron and hole spin states are shown for two orthogonal orientations of the magnetic field when in the plane of the sample. The possible transitions between these states and their optical polarization states are indicated by the vertical arrows and the transitions are numbered to facilitate the discussion of the observed selection rules.

physically nonequivalent. However, if the sample is rotated by 90° around the normal to the layer, the spectrum which was recorded before the rotation in (π,σ) geometry is now observed in (σ,π) and vice versa. In other words, there is a *combined invariance* of the spectrum under the rotation by 90° of the polarizer, the analyzer, and the sample.

The reason for this combined invariance can be understood as follows. We have shown above that the intermediate Raman states for spin flip are the heavy-hole QW excitons. For sample A, it was established earlier that the in-plane g factor of the heavy holes (which is normally very small, of the order of the Luttinger parameter, $q \simeq 0.01$) is dominated by a component induced by the in-plane strain in the present specimens and is therefore extremely anisotropic[2] such that $g_x = -g_y$. This unusual behavior implies that, if the field B is in the layer plane (001) and makes an angle ϕ with respect to [110], the Zeeman splitting between the heavy-hole states is given by $g\mu_B B$, where $g^2 = g_x^2\cos^2\phi + g_y^2\sin^2\phi = g_x^2$ and does not vary with ϕ. However, the hole pseudospin does vary, the uppermost heavy-hole state being characterized by a value of $+1/2$ when the field is along x and by $-1/2$ when it is along y. In contrast, the QW electron g factor is isotropic to within the limits of our experimental accuracy. If the sample is rotated about [001] from $B\|[110]$ to $B\|[1\bar{1}0]$, the electron states will therefore remain the same, while the heavy hole states will interchange; this is shown diagramatically in Fig. 4. As a result, if the left and right panels of Fig. 4 are compared, those transitions which proceed in (π,σ) polarization on the left, proceed in (σ,π) polarization on the right (and vice versa). It is therefore expected that, in processes involving such excitons, an interchange of σ and π accompanied by a 90° rotation of the sample will yield the same spectrum. Note that, as is clear from the above expression for g, the splitting of the hole levels does not change with angle; it is only the polarization character of the optical transitions that evolves continuously with rotation.

B. Origin of the signals

As shown in Fig. 3, the excitation profile of the electron spin-flip Raman line has two distinct maxima (which we denote by D^0SF and ESF). The process responsible for the lower-energy maximum is readily identified. By its energy, this peak corresponds to the creation of an exciton-to-impurity complex D^0X which includes three charge carriers (two electrons and one hole) which serve as the intermediate state of the Raman process. Such processes have often been observed both in bulk A_2B_6 crystals[11] and in QW's, and their mechanism is well understood.[14,16,29–35] The Raman intensity of a scattering process that involves the spin flip of a donor electron can be written in second-order perturbation theory as

$$I \propto \left| \frac{\langle \mathrm{fin}|V|\mathrm{int}\rangle\langle \mathrm{int}|V^{\dagger}|\mathrm{ini}\rangle}{(\hbar\omega - E_0 + i\Gamma/2)} \right|^2, \tag{1}$$

where ini, int, and fin represent the initial, intermediate, and final states. These are, respectively: (i) the laser photon plus a neutral donor with an electron of one spin; (ii) the D^0X complex; and (iii) the Raman photon plus the neutral donor with a reversed electron spin. V and $V^{\dagger}$ are the exciton annihilation and creation operators, $\hbar\omega$ is the laser quantum energy, E_0 is the resonance energy, and Γ is the homogeneous level width.

Qualitatively, this process can be interpreted as follows [see Fig. 5(a)]. In the initial state in a magnetic field, the electron of the neutral donor occupies the lower Zeeman sublevel (for these dilute magnetic semiconductor structures, the Zeeman splitting Δ_e is typically much greater than k_BT at liquid-helium temperatures). A laser photon is absorbed and resonantly forms the exciton-to-donor complex containing the donor electron, the photocreated electron and the photocreated hole. Since the lower electron Zeeman level was already occupied, the photocreated electron must be excited to the upper level. The hole subsequently recombines with the electron in the lower level, emitting a Raman photon having energy deficit Δ_e with respect to the laser photon. We note that a second-order process of the type described by Eq. (1) involves only light emission and absorption processes, with no transitions occurring in the intermediate state.

The linewidth of the Raman replica in the process described should depend on the uncertainties of the energy of the donor electron in the initial and final spin states. The uncertainties depend, in turn, on the lifetimes of the corresponding states. As has been established in numerous studies of semiconductor crystals containing manganese ions, the relevant lifetimes for both electrons and holes are the spin relaxation times; the electron located on the upper Zeeman level is expected to flip its spin within the picosecond time scale. Therefore the lifetime of the electron in the upper level is short, the energetic uncertainty is large, and this level [i.e., the final state of Eq. (1)] is expected to give the main contribution to the linewidth of the Raman replica. The width of the Raman line corresponds to a lifetime of 2 ps, in agreement with electron-spin relaxation times in dilute magnetic semiconductors according to Ref. 37.

The interpretation of the second process, responsible for the higher-energy peak ESF in the excitation profile (Fig. 3), is more problematic. A comparison with PL and photoluminescence excitation spectroscopy (PLE) spectra implies that the intermediate state for the ESF process is a

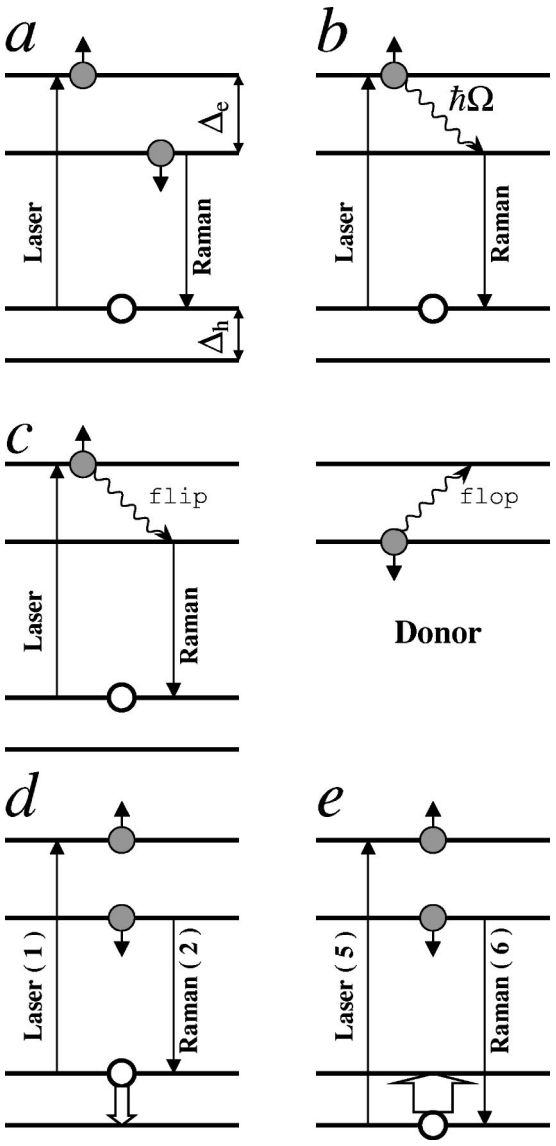

FIG. 5. Schematic representations of the possible spin flip Raman scattering processes considered in the text: (a) SFRS of a donor-bound exciton; (b) exciton spin flip with emission of an acoustic phonon; (c) spin-flip of an electron located on a remote donor; (d) and (e) SFRS of a donor-bound exciton showing the reasons for the difference in efficiency of processes 1-2 and 5-6 (Sec. III D 1).

free or weakly localized QW exciton. The Raman shift itself and the linewidth (which are both independent of the direction of the magnetic field) are the same as for excitation in the D^0X region, which suggests that the ESF Raman process also arises from the spin flip of a conduction-band electron or a shallow donor-bound electron. This supposition is supported by the similarity of the behavior of the Raman intensity in the Voigt configuration for ESF and D^0SF (see Sec. IV C).

A second-order process involving the spin flip of an electron remote from the exciton can be considered but appears to be unlikely. For example, if the QW contains excess electrons originating from donors in the barriers, the hole of the exciton may recombine with one such free electron which has a spin opposite to that of the electron in the exciton itself, in effect resulting in an electron spin flip. However, in such process, one would expect that the SFRS linewidth would be influenced by the distribution in energy of the available initial and final states occupied by the electron, whereas we observe experimentally that the Raman linewidth and shift for ESF are the same as for D^0SF. Furthermore, the efficiency of this process should depend on the concentration of electrons in the QW, which is not expected to be high in these undoped samples.

For these reasons it appears that, in order to interpret the ESF peak in the excitation profile, one has to take into account third-order processes of the form

$$I \propto \left| \frac{\langle \mathrm{fin}|V|\mathrm{int2}\rangle\langle \mathrm{int2}|P|\mathrm{int1}\rangle\langle \mathrm{int1}|V^{\dagger}|\mathrm{ini}\rangle}{(\hbar\omega - E_1 + i\Gamma_1/2)(\hbar\omega_R - E_2 + i\Gamma_2/2)} \right|^2, \qquad (2)$$

where, in addition to the creation and annihilation of the exciton, the transition between two excitonic intermediate states int1 and int2 with an accompanying flip of the electron spin is included. P stands for the operator of the corresponding perturbation, E_1 and E_2 are the incoming and outgoing resonance energies, respectively, Γ_1 and Γ_2 are the corresponding damping coefficients, and $\hbar\omega_R$ is the energy of the scattered photon. For the mechanism of the spin-flip transition between the intermediate states, we will consider two possibilities: (i) the emission of an acoustic phonon and (ii) a flip-flop process between the exciton and a remote donor.

Process (i), involving the emission of phonon, is schematically depicted in Fig. 5(b). The initial state here consists of the laser photon and the unperturbed crystal and the final state consists of the Raman photon and the crystal containing an additional phonon. Thus such a process can provide a Raman shift of Δ_e only if the energy of the created phonon equals Δ_e. In terms of Eq. (2), the internal matrix element would be $\langle e\uparrow, h\updownarrow + \hbar\Omega|c^{\dagger}|e\downarrow, h\updownarrow\rangle$, where e and h stand for the electron and hole in the exciton (arrows show their spin states) and $c^{\dagger}$ is the creation operator for a phonon of energy $\hbar\Omega$. A similar process has been envisaged by Karimov *et al.*[36] in studies of excitons strongly localized at quantum dots.

The behavior predicted on the basis of this model is somewhat different from that observed. In contrast to the D^0SF process, in the phonon-assisted Raman process the initial and final states contain no carriers and thus have comparatively long lifetimes with no contribution from spin relaxation. Therefore the main contribution to the Raman linewidth should come from the intermediate transition and should be dominated by the broadening of the first and second intermediate states. In both these states there are unpaired electrons and holes. If we assume still that the fastest decay times for charge carriers are their spin relaxation times then one can see that, apart from spin relaxation of the electron (which determines the Raman linewidth for D^0SF), the spin flip of the hole must also contribute to the broadening of both intermediate states. Since the spin-relaxation times for holes in similar QW's are, as a rule, of the same order of magnitude as for electrons or even shorter,[37] a noticeable extra broadening of the Raman line is expected compared to D^0SF.

However, experiment shows neither an extra broadening of the Raman line for ESF nor a change of the ESF Raman linewidth under the rotation of the crystal in the Voigt configuration (see Sec. IV C). On the basis of these considerations, we do not believe that the ESF resonance can be interpreted as a phonon-assisted spin flip of an electron.

The most appropriate mechanism of the ESF thus seems to be a third-order process involving the spin flip of a free electron or an electron on a remote donor [Fig. 5(c)]. For such processes, the internal matrix element in Eq. 2 may have either the form (a) $\langle e\downarrow, h\Uparrow + d\uparrow | s_d^+ s_e^- | e\uparrow, h\Uparrow + d\downarrow \rangle$ or (b) $\langle e\uparrow, h\Downarrow + d\uparrow | s_d^+ j_h^- | e\uparrow, h\Uparrow + d\downarrow \rangle$. In both cases, the right (left) intermediate state includes the donor electron d with spin along (opposite to) the field. The flip of the spin of the donor electron is accompanied by the flop (within the exciton) of the electron spin (a) or of the hole pseudospin (b); $s_d^+ s_e^-$ and $s_d^+ j_h^-$ denote the operators responsible for the corresponding flip-flop transitions. The double arrows show the direction of the hole pseudospin (we now use the pseudospin representation for holes in order to make explicit the invariability of the hole spin state in the first case and its change in the second case). Of course, matrix element (a) can equally well be written with $h\Downarrow$ on the left and right and, likewise, matrix element (b) may be written with $e\downarrow$ on the left and right. A similar mechanism has been suggested by Sapega *et al.* in the case of hole spin flip.[38]

This process can be described in the following manner. The laser photon generates a free or weakly localized exciton which further interacts with a remote donor electron causing the flip of the spin of that electron. Simultaneously the spin of the electron (or the pseudospin of the hole) in the exciton is also flipped. After that, the exciton recombines generating the Raman photon and leaving a donor electron (with flipped spin) in the crystal. This process should be resonantly enhanced when the laser is tuned to the free or weakly localized QW exciton transition energy, as is observed for ESF. The linewidth is expected to be controlled by the spin relaxation time of the electron in the donor state and is thus expected to be the same as in the case of D^0SF. The large intensity of this third-order process (comparable to that of second-order D^0SF) can be explained by the much larger density of states for free QW excitons compared to that for D^0X complexes. Therefore, in what follows, we proceed from the assumption that the observed ESF resonance originates from a third-order Raman process with a flip-flop transition in the intermediate state.

C. Angular dependences of Raman intensity in Voigt geometry

1. The D^0SF process

Now that the processes by which electron SFRS occurs have been identified, we turn to the key observation of the present paper: the dependence of the intensity of the Raman lines on the orientation of the magnetic field in the plane of the QW's. Figure 6(a) shows the dependence of the intensity of the electron spin-flip (D^0SF) recorded in (π,σ) geometry on the angle ϕ. Figure 6(b) shows the analogous dependence taken in the second ''crossed'' geometry, (σ,π). In both cases, a substantial and regular variation of the intensity by a factor of about 3 is observed. This variation cannot be attributed to any change of the optical alignment during the rotation, the more so as the quality of alignment can be easily checked by the intensity of the PL, which is only weakly polarized under these conditions.[2] One can see that the angular dependences are dominated by a 180° repeat pattern, but with the dependences for (π,σ) and (σ,π) having opposite phases. The two cases in which the field is directed along the [110] axis ($\phi=0°$) and the $[1\bar{1}0]$ axis ($\phi=90°$) (which are equivalent for an *ideal* QW having D_{2d} symmetry) are observed to give different Raman intensities, revealing the lower C_{2v} symmetry of the QW under study. This provides an important new confirmation of our previous observations.[2] The Raman intensity on the ESF resonance behaves analogously, and the angular dependences recorded in each of the crossed geometries have the same phase as those for D^0SF. We emphasize that no variation with ϕ was observed either of the Raman shift or of the Raman linewidth.

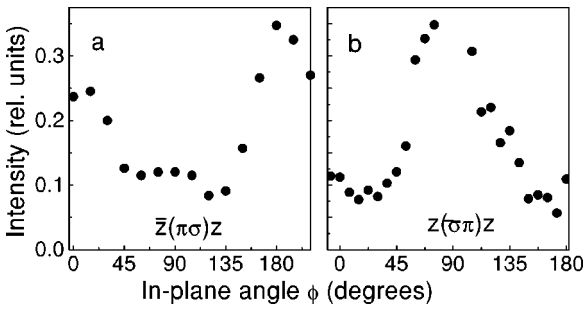

FIG. 6. (a) Dependence of the intensity of the electron spin flip (D^0SF) of sample A on the angle ϕ between the [110] direction and the magnetic field recorded in the (π,σ) geometry; (b) the analogous dependence recorded in the (σ,π) geometry.

The mechanism of such anisotropy of the spin-flip Raman intensity in QW's can be discussed on the basis of the earlier considerations. We take first the D^0SF process in the (π,σ) polarization geometry and use, for convenience, the notation of the optical transitions given in Fig. 4. We analyze first the left-hand part of that figure ($\phi=0°$). For π-polarized incoming light, the transitions considered as candidates for involvement in the SFRS process are 1 and 3 while, for σ-polarized outgoing light, they are 2 and 4. However, since the lower Zeeman component for the electron is already occupied by the electron on the (thermalized) donor, transition 3 and hence processes 3-2 and 3-4 are ruled out. Process 1-4 is also ruled out since it does not correspond to a spin flip of the donor electron. Thus for $\phi=0°$, the process must proceed via the 1-2 channel. For $\phi=90°$ (the right-hand part of Fig. 4), we find by analogous reasoning that the relevant process must be 5-6.

To explain why different Raman intensities are observed for $\phi=0°$ and for $\phi=90°$, one must therefore compare processes 1-2 and 5-6 and identify the reason for their different efficiency [see Figs. 5(d) and (e)]. This must involve the value of the Raman denominator in Eq. (1). Close to resonance $\hbar\omega \approx E_0$ and the absolute value of the denominator strongly depends on the damping coefficient Γ, which is, in

turn, inversely proportional to the lifetime of the intermediate state. As we already noted when discussing the phonon-assisted spin flip, it is reasonable to assume that the flip of hole pseudospin is one of the fastest relaxation processes and that it can determine the lifetime of the intermediate state (both electron spin states are occupied in the D^0X intermediate state, so electron spin relaxation is not relevant). In the 5-6 scheme, the decay of the higher energy hole state occurs by a transition to the lower energy level; i.e., this process proceeds with a dissipation of energy and therefore rapidly. On the contrary, in process 1-2 the decay of the hole state by a flip of the pseudospin requires an activation energy of the order of the hole Zeeman splitting, and thus proceeds at a factor of $\exp(\Delta_h/k_BT)$ more slowly. As a result, for $\phi=0°$, the decay time is longer, the Raman denominator is smaller, and the intensity of Raman scattering is higher than for $\phi=90°$. This indeed corresponds to the observations in the (π,σ) configuration. A similar argument has already been used to explain the observed difference in intensities of (π,σ) and (σ,π) SFRS,[35] though, in that work, no anisotropy of the kind discussed here was observed.

One can readily see that, for the (σ,π) configuration, the converse reasoning holds. Process 4-3 dominates for $\phi=0°$ and process 8-7 for $\phi=90°$. The latter process has the smaller Raman denominator, which accounts for the increase of the Raman intensity from $\phi=0°$ to $\phi=90°$ observed in this polarization.

2. The ESF process

For the case of the anisotropy of the intensity of the ESF Raman signal, discussion of the schemes specific to the (π,σ) geometry is sufficient in view of the combined invariance described in Sec. IV A. We use the results of Sec. IV B and propose that the ESF is a third-order process with a reciprocal flip of the spin of a donor electron and the spin of electron (or pseudospin of the hole) in the exciton. In the intermediate state, the exciton has only one electron, which can have either spin. We therefore have to consider a greater number of possibilities than in Sec. IV C 1. For $\phi=0°$, these are 1-2, 3-4, 1-4, and 3-2. However, the following considerations can help identify the most effective process.

The third-order process is expected to increase in strength the more closely double resonance conditions are fulfilled ["double resonance" implies that *both* terms in the denominator of Eq. (2) are minimized]. Due to the short spin lifetimes, the two electron and the two hole sublevels are pairs of overlapping bands rather than pairs of distinct levels so that, for example, process 3-4 can in principle proceed even with the energy of the σ transition smaller than the energy of π transition, i.e., as a Stokes process. However, such a process is very unfavorable with respect to the double resonance conditions (see Fig. 7). This reason alone makes the 1-2 process much more probable than the 3-4 process. The same holds for the pair of transitions involving a hole flip, where the double resonance enhances process 3-2 with respect to process 1-4. By comparing processes 1-2 and 3-2 and setting aside differences in matrix elements, process 1-2 is likely to be stronger because, in this process, the double resonance conditions can be satisfied exactly, while in 3-2 they are not

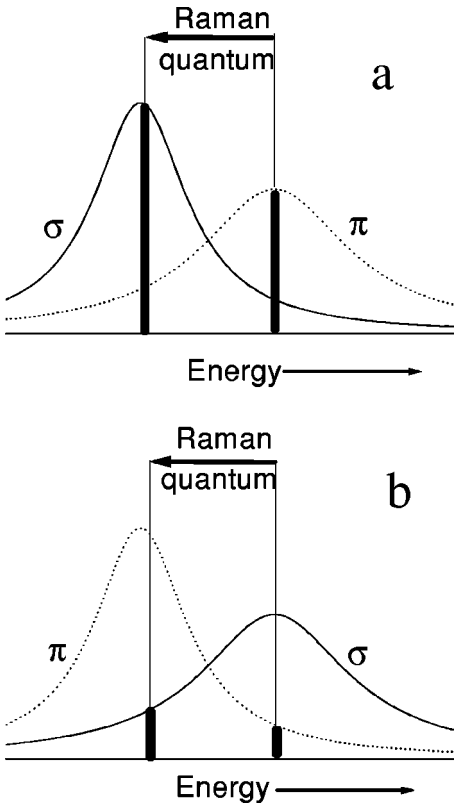

FIG. 7. A representation of the broadened intermediate states involved in the Stokes (π,σ) spin-flip process; (a) doubly resonant scattering via, e.g., process 1-2, in which excitation and emission are at the maxima of the bands centered at each electron spin sublevel; (b) scattering via, e.g., process 3-4, where double resonance conditions are poorly satisfied.

because the hole sublevel splitting is in general different from the splitting of the donor electron.

We therefore conclude that, for $\phi=0°$, the main channel should be process 1-2. Analogously, for $\phi=90°$, process 5-6 should dominate. The situation is then equivalent to the D^0SF case considered above, which explains the observation that the angular dependences of the intensities of the D^0SF and ESF signals are in phase and have similar amplitudes. However, it is worth noting that the predicted phase of the angular dependence for ESF is not altered if processes 3-2 (for $\phi=0°$) and 5-8 (for $\phi=90°$) also contribute.

In summary, the anisotropic lateral g factor of the holes, together with the concept that it is the fast hole spin relaxation that limits the lifetime of the intermediate Raman state, allows us to explain the observed angular dependence of the intensity of the electron spin-flip signal, the reversal of the phase of this dependence on reversal of the polarization geometry and the similarity of the angular dependences for the ESF and D^0SF resonances. The explanation is consistent with the conclusions about the origin of those resonances derived in Sec. IV B.

D. Reconstruction of the hole *g* tensor

By comparing the processes 1-2 and 5-6 proposed to be responsible for the electron spin flip for angles $\phi=0°$ and

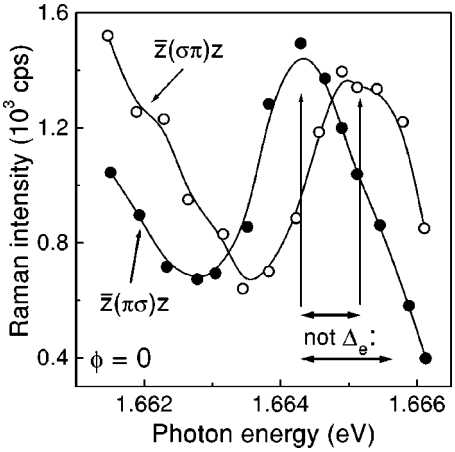

FIG. 8. Excitation profiles for the electron spin-flip scattering of sample A at a magnetic field of 4 T in the Voigt (σ,π) and (π,σ) geometries (open and filled circles, respectively) with $\phi=0$. The solid lines are guides to the eye. The vertical arrows indicate the positions of the peaks of the resonance profiles in the energy region of the quantum well exciton (''*X*'') transitions. Upper horizontal arrow: the measured splitting of the resonance profiles; lower horizontal arrow: the electron spin splitting measured via SFRS at 4 T.

$\phi=90°$ respectively, another prediction may be made. This is that the 1-2 process will be resonant at an excitation energy corresponding to the energy splitting of the upper hole and upper electron sublevels, $E_0=E_X(B=0)+(\Delta_e-\Delta_h)/2$, where $E_X(B=0)$ is the energy of the exciton in zero magnetic field while, for the 5-6 process, resonance will be at the energy splitting of the lower hole and upper electron sublevels $[E_0=E_X(B=0)+(\Delta_e+\Delta_h)/2]$. This implies that electron spin-flip excitation profiles taken in the same geometry at $\phi=0°$ and $\phi=90°$ should be shifted relative to each other by an amount equal to the hole sublevel separation Δ_h. The same also applies to the profiles taken at one value of the angle ϕ but in opposing polarization geometries (this is the combined invariance discussed in Sec. IV A).

Experiment shows that this prediction is correct (Fig. 8). At $\phi=0°$ the resonance profile for (σ,π) (process 4-3) is shifted toward higher energies as compared to the profile for (π,σ) (process 1-2). The value of the shift amounts to 0.85 meV at $B=4$ T. This observation leads us to reconsider briefly the interpretation of the angular dependences in the previous subsection. The shift of the resonance profiles must contribute to the angular variation of the Raman intensity recorded at a fixed laser energy. However, this shift is small compared to the width of the profiles and thus it cannot be the principal reason for the variation of intensity by a factor of 3 (as shown in Fig. 6).

The shift of the profiles in Fig. 8 yields the first estimate of the value of the hole splitting arising from the extremely anisotropic in-plane *g* factor of holes in this QW. The previous measurements of the polarization of the luminescence[2] only revealed the form of the hole *g* tensor, while the actual values of the in-plane components remained unknown. The in-plane *g*-factor components turn out to be surprisingly large, so that the splitting Δ_h is only slightly less than Δ_e (which is known from the Raman shift and which is 1.35 meV at 4 T). This similarity of the values of the electron *g* factor and the transverse hole *g* factor also manifests itself in the results on manganese spin flip (Sec. V).

We note that to attempt to determine the hole in-plane *g* factor from the splitting $\Delta_h=0.85$ meV at a field of 4 T would be incorrect, as the value of Δ_h contains a contribution from the ''exchange field'' produced by the manganese magnetization which, at 4 T, already tends to saturation. At the same time, at a smaller field the experimental determination of Δ_h becomes more imprecise because of its small size compared to the width of the resonance profiles. We therefore account for the saturation by considering the dependence of the electron Raman shift on the external field (see Fig. 2). For example, at 1 T, where the magnetization is still linear in the external field, the value of Δ_e is 0.7 meV; at 4 T Δ_e is 1.35 meV, that is, the exchange field for $B=4$ T is a factor of 1.93 larger than at $B=1$ T. Thus, the value of Δ_h scaled to 1 T is $0.85/1.93=0.44$ meV. Since at $B=1$ T the magnetization is linear in *B*, the value of the hole *g* factor follows from the relation $\mu_B g_{h\perp}=\Delta_h/B=0.44$ meV/T $(g_{h\perp}=|g_x|=|g_y|=7.7)$. However, the most interesting and physically meaningful quantity is not so much the absolute value of the exchange-enhanced transverse (in-plane) hole *g* factor but its value relative to the longitudinal hole *g* factor.

The longitudinal *g* factor was derived from the magnetic field-induced redshift of the excitonic luminescence lines in the Faraday geometry. The doubled value of the shift yields $\Delta_e+\Delta_h=3.2$ meV at $B=1$ T and, by subtracting $\Delta_e=0.7$ meV, one obtains an estimate of the longitudinal hole *g* factor in the form $\mu_B g_{h\parallel}=\Delta_h/B=2.5$ meV/T $(g_{h\parallel}=43)$. In addition, the value of $g_{h\parallel}$ determined in this way was used in an analysis of the angle-dependent redshifts of the excitonic luminescence line observed in the tilted magnetic field configurations between Faraday and Voigt in accord with the relation

$$\Delta_h(\theta)=\mu_B B\sqrt{g_{h\perp}^2\sin^2\theta+g_{h\parallel}^2\cos^2\theta} \tag{3}$$

(with $\theta=0°$ corresponding to the Faraday and $\theta=90°$ to the Voigt geometry). From this, we find that $\mu_B g_{h\perp}=0.45$ meV/T, in excellent agreement with the value 0.44 meV/T obtained from the excitation profiles.

The set of measurements described therefore allows the complete reconstruction of the effective hole *g* tensor in a specific QW. For the present sample, this tensor (in its principal axes) takes the form

$$\hat{g}_h=\begin{pmatrix}43&0&0\\0&7.7&0\\0&0&-7.7\end{pmatrix}=A_h\begin{pmatrix}3&0&0\\0&0.54&0\\0&0&-0.54\end{pmatrix}, \tag{4}$$

where, following Ref. 2, we define the longitudinal component of the unenhanced *g* tensor to be 3; A_h stands for the factor of the exchange enhancement of the external magnetic field due to its indirect action on the hole mediated by the manganese spins. The tensor expressed using A_h presents an important estimate of the value of the lateral hole *g* factor

(independent of effects due to the Mn^{2+} magnetization) which can be induced in QW's by an in-plane strain.

V. MANGANESE SPIN FLIP

In QW's containing semi-magnetic well layers, multiple light-scattering processes involving $3d^5$ manganese electrons have been observed in the Voigt configuration and more than 15 peaks have been reported.[39–41] A semi-classical theory of this phenomenon has been developed involving the collective precession of the manganese spins in the exchange field of the localized hole.[39,40] In our QW's, the exciton-to-manganese coupling is evidently weaker (Mn^{2+} ions are in the barrier layers only), and a smaller number of peaks is observed. In what follows we shall examine in detail only the first Stokes (1S) and the first anti-Stokes (1AS) manganese spin-flip peaks; these both have a large intensity and, having the smallest Raman shift, do not overlap with other spectral features.

The flip of a single manganese $3d^5$-electron spin (referred to as MnSF) can be naturally considered as a third-order process.[1,34] This process is described by Eq. (2) and is in many respects analogous to the ESF processes. It was proposed above that, for ESF, the dominant mechanism involves an electron-electron flip-flop transition in the intermediate state. Bearing in mind, on the one hand, the similarities of MnSF with ESF and, on the other hand, its interpretation on the basis of the hole-manganese interaction,[39,40] we shall address the question of which particle within the exciton (electron or hole) is responsible for flipping the Mn spin.[28]

A. Excitation profiles and angular dependences

The MnSF excitation profiles, like the electron spin-flip excitation profiles, embrace two regions of the QW PL spectrum: the excitonic region (process XMnSF) and the D^0X complex region (process D^0MnSF). In sample B, the D^0MnSF resonance manifests itself as a distinct peak in the profile, along with XMnSF. In sample A, the XMnSF efficiency is much higher than that of D^0MnSF, so the latter does not yield a distinct peak and forms a low-energy shoulder on the XMnSF resonance which is more or less pronounced in different polarizations (Fig. 3). Judging by the PL spectra and the electron spin-flip profiles, the concentration of donors in sample B is few times higher than in sample A.

Figures 9(a) and (b) show the angular dependences (in the Voigt configuration) of the intensities of the 1S XMnSF and 1S D^0MnSF signals for sample B together with those of the respective electron spin-flip signals (ESF and D^0SF). The angular dependence for 1S XMnSF has the same phase as ESF, though with a somewhat weaker amplitude. The 1S D^0MnSF shows a much more pronounced angular dependence which, moreover, has the opposite phase to the electron spin flip. Similar behavior is observed for the 1S D^0MnSF signal in sample A.

The fact that the angular dependences for D^0SF and 1S D^0MnSF [Fig. 9(a)] are in antiphase can be explained by use of the schemes of Fig. 4. It was shown in Sec. IV C 1 that in (π,σ) the second-order D^0SF process occurs via the 1-2 path (for $\phi=0°$) or via 5-6 (for $\phi=90°$), the 1-2 mechanism leading to the higher intensity. The third-order D^0MnSF process contains the intermediate flip-flop transition in which the paired electrons of the D^0X complex cannot take part. Obviously, the manganese spin can be flipped only by interaction with the hole. The incoming transition involving the lower electron sublevel is essentially blocked at low temperatures. Furthermore, since the spin flip of the donor electron does not contribute to the Raman shift for the process under discussion, it is evident that the spin state of the donor electron is unchanged as a result of the process. Therefore an outgoing transition from the lower electron sublevel is ruled out and the MnSF Raman process can only proceed through the upper sublevel: all the transitions of Fig. 4 are thus ruled out with the exceptions of 1-4 (for $\phi=0°$) and 5-8 (for $\phi=90°$). These two processes are similar with respect to decay times, since the same sublevels are involved in both (only the first and second intermediate states exchange their places). The double resonance conditions are evidently better satisfied for 5-8 than for 1-4 (see Fig. 7). As a consequence, the angle where the D^0SF intensity is the largest ($\phi=0°$) gives the smallest intensity of 1S D^0MnSF.

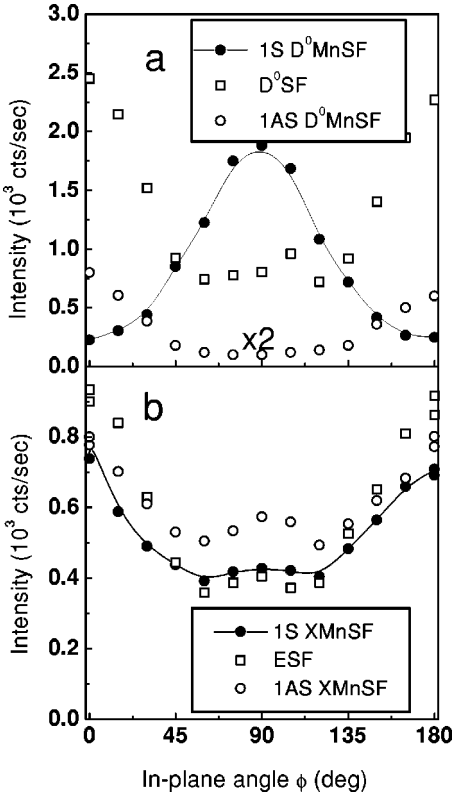

FIG. 9. Angular dependences (in the Voigt geometry) of the intensities of the Mn^{2+} spin-flip Raman signals of sample B in resonance with (a) the donor bound exciton (D^0MnSF; filled circles: Stokes; open circles: anti-Stokes) and (b) the quantum well exciton (XMnSF; symbols as above) for sample B together with those of the corresponding electron spin-flip signals (D^0SF and ESF respectively; open squares). The lines are guides to the eye.

The same argument explains also the observation [Fig. 9(a)] that the 1S and 1AS D^0MnSF lines exhibit opposite dependences on the angle ϕ. If the hole is to be responsible

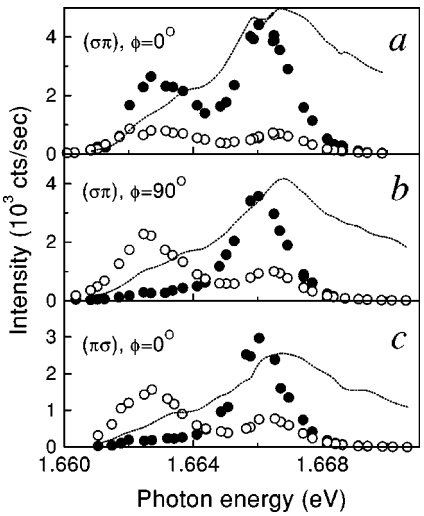

FIG. 10. The resonance profiles, in three different geometries, of the electron spin-flip (open circles) and manganese spin-flip (filled circles) signals of sample B. The solid line shows the photoluminescence excitation spectrum.

for the Mn spin flip, both 1S and 1AS D^0MnSF can only proceed via the process 1-4 of Fig. 4 when, for example, $\phi = 0°$. The double resonance conditions are satisfied better for anti-Stokes scattering via process 1-4 (which represents the ideal anti-Stokes pair of transitions) and worse for Stokes scattering.

We emphasize that it is the blocking of transitions involving the lower electron sublevel in the D^0MnSF process that is responsible for the antiphase behavior of D^0SF and 1S D^0MnSF, by forcing the latter process to proceed, in a given geometry, via the path which is unfavorable with respect to the double resonance conditions. The same argument accounts for the large variation in intensity of the 1S D^0MnSF signal with ϕ shown in Fig. 9. Naturally, for 1S XMnSF no blockade is expected and thus the manganese spin-flip intensity should exhibit different behavior on the X and the D^0X resonances.

This is illustrated by the data shown by solid circles in Figs. 9(a) and (b) and is also shown by the excitation profiles of the electron and 1S manganese spin-flip signals taken in three different geometries [Figs. 10(a)–(c)]. On this figure, the left- and right-hand peaks of each profile are in resonance with the D^0X and X states, respectively. Whereas the electron spin-flip resonances ESF and D^0SF (open circles) and the 1S XMnSF resonance all show a similar variation of intensity from one geometry to another, independent of which resonance is considered, the 1S D^0MnSF peak becomes much weaker in those polarization geometries [Figs. 10(b) and (c)], where it is forced to proceed against the double resonance conditions.

Figure 11 shows the behavior of the XMnSF Stokes and anti-Stokes resonance profiles at a series of magnetic fields. Figure 11(a) shows the excitation profiles for the 1S and 1AS signals of sample A in fields of 2, 4, and 6 T at $\phi = 0°$ in the (π,σ) geometry. In Fig. 11(b), the profiles taken in the (σ,π) geometry are plotted. Two qualitative differences can be seen: (i) in (π,σ), the 1S and 1AS profiles are centered at

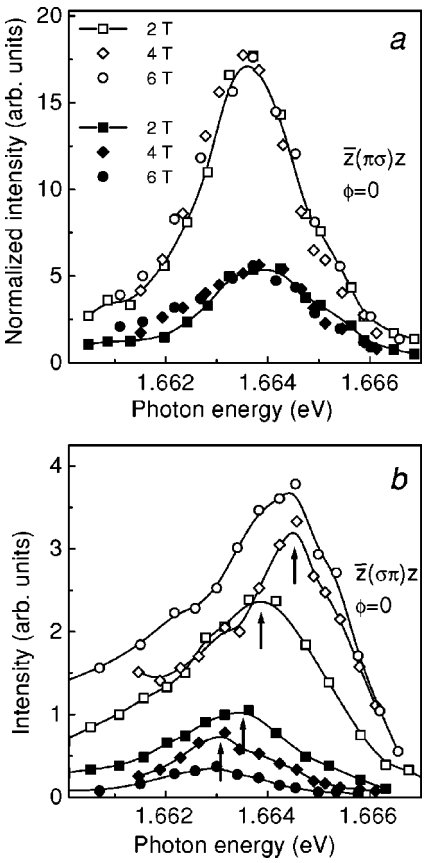

FIG. 11. Excitation profiles of the Stokes and anti-Stokes Mn^{2+} spin-flip Raman signals for sample A (open and filled symbols, respectively) at fields of 2, 4, and 6 T (squares, diamonds, and circles) in (a) the (π,σ) and (b) the (σ,π) configurations in the Voigt geometry with $\phi = 0$. The lines are guides to the eye. The vertical arrows in (b) indicate the movement of the peak positions of the resonances.

one energy while in (σ,π) the 1AS maximum is shifted toward lower energy with respect to the 1S maximum; (ii) in (π,σ), the maxima do not move noticeably with increasing field while in (σ,π) the 1AS maximum shifts toward lower energies and the 1S maximum toward higher energies.

The same line of reasoning as in Sec. IV C 2 clarifies these results. For 1S XMnSF one can reject half of the possible schemes due to the unfavorable double resonance conditions, so that for (π,σ) the alternative processes 1-2 or 3-2 will remain while for (σ,π), they are 4-3 or 4-1. Analogously, for 1AS XMnSF in (π,σ) either 3-4 or 1-4 will dominate and, in (σ,π), either 2-1 or 2-3. In all four sets of transitions mentioned, the first process involves an electron flip (and manganese), and the second, a hole flip (and manganese). While in the case of ESF, additional reasons led us (Sec. IV B) to propose electron-electron flip flops compared to hole-electron ones, in the case of XMnSF it is difficult to identify *a priori* electron or hole. In principle, the hole interacts with manganese somewhat more strongly,[30] but its wave function penetrates less into the barriers because of the heavier hole effective mass.

Neither are we able to discriminate between hole and electron processes in XMnSF on the basis of the data of Fig.

11, as the behavior of the SFRS profiles can be explained qualitatively by either process. We consider here only the electron process, since a discussion in terms of the hole is similar. The key to the explanation is, again, the layout of the spin sublevels for $\phi=0°$ (Fig. 4) and the closeness of the values of the electron- and the in-plane-hole g factors (see Sec. IV D). In the (π,σ) geometry, processes 1-2 and 3-4 are responsible for Stokes and anti-Stokes scattering, respectively. For process 1-2, the incoming π photon induces the transition between the upper hole and the upper electron spin sublevels (transition 1); the energy gap between these sublevels in the magnetic field is $E_X(B=0)+(\Delta_e-\Delta_h)/2$, which, when $\Delta_e\approx\Delta_h$, does not differ significantly from $E_X(B=0)$. The same holds for transition 3 in the 3-4 scheme [incoming resonance $E_X(B=0)+(\Delta_h-\Delta_e)/2$]. In total, this predicts the coincidence of the 1S and 1AS maxima and the absence of any shift in them with increasing field [Fig. 11(a)]. In (σ,π) the situation is different: the Stokes scattering is accounted for by 4-3 [incoming resonance $E_X(B=0)+(\Delta_e+\Delta_h)/2$] and the anti-Stokes by 2-1 [incoming resonance $E_X(B=0)-(\Delta_e+\Delta_h)/2$]. Obviously, when the field is increased, the 1S signal will now shift toward higher energies while the 1AS will shift towards lower energies [Fig. 11(b)].

According to the above reasoning, the separation between the 1S and 1AS maxima in (σ,π) at a given field (e.g., 1.5 meV at 4 T) should equal the sum of the electron and hole splittings. In fact the sum is larger (1.35 meV for the electron, from the Raman shift of ESF, plus 0.85 meV for the hole, from the shift of the ESF profiles, yields 2.2 meV). A similar result is the low-energy shift of the 1S XMnSF profile by 0.6 meV with respect to the ESF profile for $B=2$ T in (π,σ) [see Fig. 3; the same was observed in (σ,π)]. Looking at the schemes of Fig. 4, one can suppose that the ESF proceeds via process 1-2 while the 1S XMnSF proceeds via process 3-2, so that the difference of electron and hole g factors is responsible for the observed shift. However, quantitatively the shift is too large to explain in this way only. Apparently, both the separation of the 1S and 1AS signals and the shift of the manganese profile compared to the electron profile are influenced by another important factor. The 1S XMnSF is a double resonance process, and this double resonance is always frustrated in the sense that due to the difference of g factors of electron (or hole) and manganese, the flip of the latter is not energetically counterbalanced by the flop of the former. This distinguishes 1S XMnSF from ESF, for which the exact incoming resonance is, at the same time, always the exact outgoing resonance. The example of D^0MnSF showed how strong the influence of double resonance conditions is on the manganese spin flip. Thus it is quite natural that the MnSF profile will always shift from the exact incoming resonance toward the exact outgoing resonance. In particular, even if one suggests that ESF and 1S XMnSF proceed through the same scheme (1-2), the optimal conditions of observation of these processes (the maxima of the profiles) will have different spectral positions, with 1S XMnSF being at lower energy as in Fig. 3. As a result, the shifts of the manganese profiles discussed also do not allow us to discriminate between electrons or holes as the main agent for the manganese spin flip in the XMnSF process.

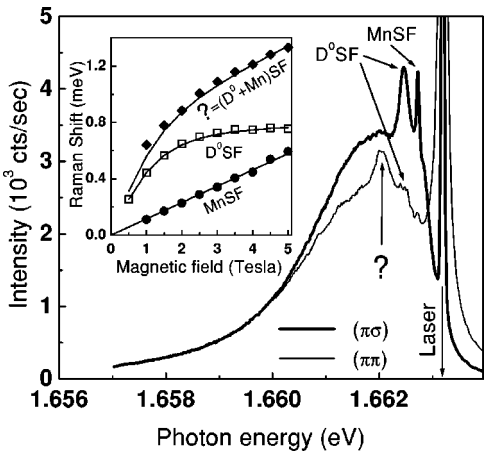

FIG. 12. Spectra for sample B showing the new line (marked ?) observed in the (π,π) geometry with $\phi=90°$ together with the MnSF and D^0SF lines already discussed. A spectrum obtained under similar conditions in the (π,σ) geometry is shown for comparison (heavy line). The inset shows the dependence of the Raman shifts of these three lines on magnetic field together with fitted curves (solid lines) as described in the text.

VI. COMBINED ELECTRON AND MANGANESE SPIN FLIPS

The results presented so far are concerned with the signals observed in the (σ,π) and (π,σ) geometries. In the geometries (π,π) and (σ,σ) for $\phi=90°$ and $\phi=0°$, respectively, a new line was observed [it is not observed, for example, for $\phi=0°$ in the (π,π) geometry]. We shall show here that the existence, intensity, and polarization properties of this line are predicted by the model proposed here for all the SFRS processes and its observation therefore provides further confirmation of the model.

A representative spectrum is shown in Fig. 12 together with its dependence on magnetic field (inset; diamonds) and a curve (inset; solid) constructed by adding the Brillouin function fit to the magnetic-field dependence of the electron spin-flip signal to a linear Zeeman splitting with a g factor of 2. The behavior of this new signal is very well described by the constructed curve and the line is therefore assigned to the combination of a flip of an electron and a Mn^{2+} internal transition, as also recently observed in (Ga,Mn)As.[42] No shift of this line was observed on rotation of the sample normal with respect to the magnetic field (that is, variation of the angle θ), though it rapidly became weaker. These two facts indicate that the alternative explanation of this line as the combined flip of an electron and a hole within an exciton (as discussed in Ref. 36 for excitonic scattering) can be ruled out. This latter process (which is the phonon-assisted process discussed in Sec. IV B) would have a highly anisotropic splitting with respect to the rotation θ, since a contribution to the splitting from the relatively large hole g factor $g_{h\|}$ is introduced when $\theta\neq\pi/2$ [see Eq. (3)].

The detailed predictions of the model for this line are as

follows. We start from the mechanism for D^0MnSF established in Sec. V. In the $\phi = 0°$ geometry, the process most closely satisfying double resonance conditions is 4-1 (Fig. 4). If, however, the recombination of the hole is with the other electron (both electron sublevels are occupied), corresponding to the process 4-2, then a combined flip of the donor and manganese electrons has resulted. For $\phi = 90°$ (the experimental conditions of Fig. 12, the combined process analogous to 4-2 is 5-7.

The combined spin-flip process is therefore an *inevitable* consequence of the present model, since the only distinction between the combined process and, for instance, a single Mn^{2+} flip via interaction with the hole state is the question of which electron state the hole recombines with. The combined process is therefore expected to have a strength (in the appropriate geometry) which is comparable to that of the single flip; this is as observed (Fig. 12). Finally, the polarization properties of the combined line are also predicted correctly. Referring again to Fig. 4, the polarizations of the two processes 4-2 and 5-7 are (σ,σ) and (π,π), respectively, as is indeed observed.

VII. CONCLUSIONS

We have studied CdTe/$Cd_{1-x}Mn_x$Te quantum wells with an in-plane anisotropy via spin-flip Raman scattering. Three spin-flip Raman-scattering signals were observed (electron Stokes and manganese Stokes and anti-Stokes), each having different behavior depending on the resonant intermediate state (a localized QW exciton or a donor-bound exciton), and the mechanisms of the scattering processes have been identified.

A dependence of the spin-flip Raman intensity on the orientation of the crystal with respect to the magnetic field in the Voigt configuration was observed and was interpreted in terms of spin-flip Raman scattering with various excitonic spin states serving as intermediate states. The existence of an extremely anisotropic in-plane hole *g* factor in these samples that was previously reported[2] was thus confirmed and this anisotropy has been quantified in the present work by two means which provide estimates in good agreement with one another.

The anisotropic hole *g* factor is not only a phenomenon which results in specific polarization properties of luminescence and spin-flip Raman spectra, but is also valuable as a tool allowing one to manipulate the Raman intermediate states by variation of the polarization geometry of the experiment and of the Voigt angle ϕ. By these means, detailed information on the mechanisms of spin-flip Raman scattering was obtained. In particular, we have shown that the electron spin-flip processes that proceed via purely excitonic states (ESF) involve electron-to-electron flip-flops in the intermediate state while the manganese spin-flip processes that proceed via D^0X states (D^0MnSF) involve hole-to-manganese flip flops in the intermediate state. This model leads to detailed predictions concerning the existence, intensity, and polarization properties of the process involving the combined spin flip of donor-bound and manganese electrons, all of which were confirmed experimentally.

ACKNOWLEDGMENTS

D.W., Y.K. and A.K. gratefully acknowledge the support of the Royal Society for this work. The work in Poland was supported by the European Commission by contract ICA1-CT-2000-70018 (Center of Excellence CELDIS). The work in Russia was partially supported by the Russian Foundation for Basic Research (00-02-16941 and 01-02-17906) and Ministry of Science and Technology (01.40.01.09.03).

*URL: http://staff.bath.ac.uk/pysdw
electronic address: d.wolverson@bath.ac.uk

[1] A. K. Ramdas and S. Rodriguez in *Diluted Magnetic Semiconductors*, edited by J. Furdyna and J. Kossut, Semiconductors and Semimetals Vol. 25, edited by R. K. Willardson and A. C. Beer (Academic, New York, 1988), pp. 345–412.

[2] Yu. G. Kusrayev, A. V. Koudinov, I. G. Aksyanov, B. P. Zakharchenya, T. Wojtowicz, G. Karczewski, and J. Kossut, Phys. Rev. Lett. **82**, 3176 (1999).

[3] H. W. van Kesteren, E. C. Cosman, W. A. J. A. van der Poel, and C. T. Foxon, Phys. Rev. B **41**, 5283 (1990).

[4] C. Gourdon and P. Lavallard, Phys. Rev. B **46**, 4644 (1992).

[5] O. Krebs and P. Voisin, Phys. Rev. Lett. **77**, 1829 (1996).

[6] L. Vervoort, R. Ferreira, and P. Voisin, Phys. Rev. B **56**, R12 744 (1997).

[7] A. V. Platonov, V. P. Kochereshko, E. L. Ivchenko, G. V. Mikhailov, D. R. Yakovlev, M. Keim, W. Ossau, A. Waag, and G. Landwehr, Phys. Rev. Lett. **83**, 3546 (1999).

[8] R. I. Dzhioev, H. M. Gibbs, E. L. Ivchenko, G. Khitrova, V. L. Korenev, M. N. Tkachuk, and B. P. Zakharchenya, Phys. Rev. B **56**, 13 405 (1997).

[9] A. Kudelski, A. Golnik, J. A. Gaj, F. V. Kyrychenko, G. Karczewski, T. Wojtowicz, Yu. G. Semenov, O. Krebs, and P. Voisin, Phys. Rev. B **64**, 045312 (2001).

[10] J. Domagala, J. Bak-Misiuk, J. Adamczewska, Z. R. Zytkiewicz, E. Dynowska, J. Trela, D. Dobosz, E. Janik, and M. Leszczynski, Phys. Status Solidi A **171**, 289 (1999).

[11] G. D. Thomas and J. J. Hopfield, Phys. Rev. **175**, 1021 (1968).

[12] P. A. Fleury and J. F. Scott, Phys. Rev. B **3**, 1979 (1971).

[13] R. Ebert, H. Pascher, G. Appold, and H. G. Hafele, J. Appl. Phys. **14**, 155 (1977).

[14] Y. Oka and M. Cardona, Phys. Rev. B **23**, 4129 (1981).

[15] S. Geschwind and R. Romestain, in *Light Scattering in Solids*, edited by M. Cardona and G. Güntherodt, Topics in Applied Physics Vol. 54 (Springer, Berlin, 1984).

[16] J. F. Scott, Phys. Rep. **194**, 379 (1990).

[17] X. C. Zhang, S. K. Chang, A. V. Nurmikko, L. A. Kolodziejski, R. L. Gunshor, and S. Datta, Phys. Rev. B **31**, 4056 (1985).

[18] H. Mariette, F. Dal'bo, N. Magnea, G. Lentz, and H. Tuffigo, Phys. Rev. B **38**, 12 443 (1988).

[19] S. R. Jackson, J. E. Nicholls, W. E. Hagston, T. J. Gregory, P. Harrison, B. Lunn, and D. E. Ashenford, Superlattices Microstruct. **12**, 447 (1992).

[20] K. Kheng, R. T. Cox, Y. Merle d'Aubigné, F. Bassani, K. Sami-

nadayar, and S. Tatarenko, Phys. Rev. Lett. **71**, 1752 (1993).
[21] K. Kheng, R. T. Cox, V. P. Kochereshko, K. Saminadayar, S. Tatarenko, F. Bassani, and A. Franciosi, Superlattices Microstruct. **15**, 253 (1994).
[22] R. C. Miller, A. C. Gossard, W. T. Tsang, and O. Munteanu, Solid State Commun. **43**, 519 (1982).
[23] M. Kutrowski, K. Kopalko, G. Karczewski, T. Wojtowicz, and J. Kossut, Thin Solid Films **267**, 64 (1995).
[24] M. P. Halsall, S. V. Railson, D. Wolverson, J. J. Davies, B. Lunn, and D. E. Ashenford, Phys. Rev. B **50**, 11 755 (1994).
[25] D. L. Peterson, A. Petrou, M. Dutta, A. K. Ramdas, and S. Rodriguez, Solid State Commun. **43**, 667 (1982).
[26] R. Meyer, G. Schaack, and A. Waag, Mater. Sci. Forum **463**, 1822 (1995).
[27] M. Hirsch, R. Meyer, and A. Waag, Phys. Rev. B **48**, 5217 (1993).
[28] J. Stühler, M. Hirsch, G. Schaack, and A. Waag, Phys. Rev. B **49**, 7345 (1994).
[29] R. Romestain, S. Geschwind, G. E. Devlin, and P. A. Wolff, Phys. Rev. Lett. **33**, 10 (1974).
[30] J. A. Gaj, R. Planel, and G. Fishman, Solid State Commun. **29**, 435 (1979).
[31] D. Heiman, P. A. Wolff, and J. Warnock, Phys. Rev. B **27**, 4848 (1983).
[32] D. L. Alov, S. I. Gubarev, and V. B. Timofeev, Zh. Éksp. Teor. Fiz. **86**, 1124 (1984) [Sov. Phys. JETP **59**, 658 (1984)].
[33] S. M. Ryabchenko and Yu. G. Semenov, Phys. Status Solidi B **134**, 281 (1986).
[34] D. Scalbert, A. Mauger, J. A. Gaj, J. Cernogora, M. Nawrocki, and C. Benoit a la Guillaume, Phys. Rev. B **43**, 7109 (1991).
[35] S. I. Gubarev, T. Ruf, and M. Cardona, Phys. Rev. B **43**, 14 564 (1991).
[36] O. Z. Karimov, D. Wolverson, J. J. Davies, T. Ruf, and L. N. Tenishev, Phys. Status Solidi B **215**, 373 (1999).
[37] S. A. Crooker, D. D. Awshalom, J. J. Baumberg, F. Flack, and N. Samarth, Phys. Rev. B **56**, 7574 (1997).
[38] V. F. Sapega, T. Ruf, M. Cardona, K. Ploog, E. L. Ivchenko, and D. N. Mirlin, Phys. Rev. B **50**, 2510 (1994).
[39] J. Stühler, G. Schaack, M. Dahl, A. Waag, G. Landwehr, K. V. Kavokin, and I. A. Merkulov, Phys. Rev. Lett. **74**, 2567 (1995).
[40] K. V. Kavokin and I. A. Merkulov, Phys. Rev. B **55**, R7371 (1997).
[41] I. I. Reshina, S. V. Ivanov, D. N. Mirlin, A. A. Toropov, A. Waag, and G. Landwehr, Phys. Rev. B **64**, 035303 (2001).
[42] V. F. Sapega, T. Ruf, and M. Cardona, Phys. Status Solidi B **226**, 339 (2001).